

Theoretical study of the photoionization of metastable neon*

A. U. Hazi and T. N. Rescigno

*Theoretical Atomic and Molecular Physics Group, University of California, Lawrence Livermore Laboratory,
P. O. Box 808, Livermore, California 94550*

(Received 28 June 1977)

We have calculated the photoionization cross section for the $(1s^2 2s^2 2p^5 3s)^3P$ metastable state of neon using *ab initio*, many-electron wave functions in the *LS*-coupling scheme. We have considered all the channels which arise from the $(1s^2 2s^2 2p^5)^2P$ state of Ne^+ and an ejected *p* electron. The continuum was made discrete by approximating the final states as superpositions of square-integrable configurations. The Stieltjes moment-theory technique was used to construct the continuum oscillator strength distribution. Both the dipole-length and the dipole-velocity forms of the cross section were evaluated. We have examined systematically the effects of orbital relaxation, core polarization, and electron correlation and found them to be important within 5 eV of threshold. The peak value of the photoionization cross section for metastable Ne is $1.9 \times 10^{-19} \text{ cm}^2$, which is much smaller than the corresponding value for the ground state. We have also calculated the line strengths for a few bound-bound transitions as well as the static polarizability of the 3P metastable state.

I. INTRODUCTION

There is a growing interest in the study of excited-state photoionization, due in large part to the importance of such processes in determining the overall efficiency that can be realized in many short-wavelength gaseous lasers. The production of photoelectrons from an excited species, which may be either the upper laser level itself or some metastable species which feeds this level, must be considered as a potentially serious loss mechanism in any system where the laser photons are sufficiently energetic to ionize the excited species in question. This will typically be the case in rare-gas excimer systems such as Kr_2^* or Xe_2^* , where photoionization plays an important role.¹

With the exceptions of atomic hydrogen,² helium³⁻⁵ and the alkali metals,⁶ the literature contains very few previous theoretical studies of *excited-state* photoionization. In the case of helium, close-coupling,³ Green's function,⁴ and complex coordinate⁵ techniques have been applied to the photoionization of the $n=2$ metastable states. In the case of the alkali metals,⁶ most theoretical work has concentrated on the nonhydrogenic behavior of the cross section, especially near threshold. Quite recently McCann and Flannery⁷ have looked at the photoionization of the 3P metastable states of the noble gases. However, these calculations were performed with one-electron model potentials which involved local approximations to the exchange interactions and averages over the several possible angular-momentum couplings between the 2P core and the ejected electron with $l=1$. In addition, neither core polarization nor correlation effects were considered in their study. Independently, Hartquist⁸ has recently examined the photo-

ionization of metastable rare gases near threshold using quantum defect theory. In this study, the cross sections were calculated using hydrogenic or Whittaker functions with experimental quantum defects.

In the present work, we have calculated the photoionization cross section for the $(1s^2 2s^2 2p^5 3s)^3P$ metastable state of Ne using *ab initio* many-electron wave functions, in the *LS* coupling scheme, to describe both the initial bound state and the final continuum states. We have considered all possible open channels which arise from a $(1s^2 2s^2 2p^5)^2P$ core and an ejected *p* electron. The continuum was made discrete by approximating the final wave functions as superpositions of square-integrable configurations. We used the recently devised Stieltjes moment-theory technique⁹ to construct the continuum oscillator strength distribution from the calculated pseudo-spectra of discrete transition energies and oscillator strengths. Since the Stieltjes imaging procedure only requires power moments of the oscillator strength distribution, which can be obtained solely from calculations in finite Hilbert space, we have been able to examine systematically the effects of electron correlation in considerable detail, without having to construct coupled-channel continuum eigenstates explicitly.

The outline of this paper is as follows. The Stieltjes moment-theory techniques are briefly summarized in Sec. II. Section III describes the calculation of wave functions and their use in constructing pseudospectra of discrete energies and oscillator strengths. The results are presented in Sec. IV. Section V contains a summary and conclusions.

II. STIELTJES MOMENT THEORY

Detailed descriptions of the Stieltjes procedures have appeared in previous publications,⁹ so only a brief summary will be given here.

The computational procedures are based upon consideration of the atomic cumulative oscillator strength distribution,

$$F(\epsilon) = \int_0^\epsilon \left[\sum_i f_i \delta(\epsilon_i - \epsilon') + g(\epsilon') \right] d\epsilon' \\ = \int_0^\epsilon df(\epsilon'), \quad (1)$$

which is uniquely determined by its power moments¹⁰

$$S(-k) = \int_0^\infty \epsilon^{-k} df(\epsilon), \quad k=0, 1, \dots \quad (2)$$

In the Stieltjes procedure,⁹ the cumulative oscillator strength is approximated by an n -term histogram of the form

$$F(\epsilon) \approx F^{(n)}(\epsilon) = \sum_{\epsilon_\alpha < \epsilon} f_\alpha, \quad (3)$$

where the n points and weights $\{\epsilon_\alpha, f_\alpha\}$, which are distinct from the correct spectrum of (1), can be obtained by solving the generalized quadrature problem associated with the specification of $2n$ values of the moments¹¹

$$S(-k) = \sum_{\alpha=1}^n \epsilon_\alpha^{-k} f_\alpha, \quad k=0, 1, \dots, 2n-1. \quad (4)$$

If the $2n$ sequential moments used in Eq. (4) are precisely those of Eq. (2), then the spectrum $\{\epsilon_\alpha, f_\alpha\}$ is said to form a *principal representation* of the oscillator strength distribution. In this case, the histogram construction of Eq. (3) rigorously bounds the correct distribution, and the values associated with the rise points,

$$\bar{F}^{(n)}(\epsilon_\alpha) = \frac{1}{2} [F^{(n)}(\epsilon_\alpha - 0) + F^{(n)}(\epsilon_\alpha + 0)], \quad (5)$$

converge to $F(\epsilon_\alpha)$ in the limit of large n .¹¹ If the moments used in Eq. (4) are not exact, as will always be the case in variational calculations on many-electron systems, the bounds of Eq. (5) will be correspondingly weakened.

The photoionization cross section is related to the continuum oscillator strength through the expression¹²

$$\sigma(\epsilon) = (2\pi/c) g(\epsilon) \quad (6a)$$

$$g(\epsilon) = \frac{dF}{d\epsilon}. \quad (6b)$$

In order to obtain this density, it is necessary to differentiate the cumulative histogram of Eq. (3)

in some fashion. Considerable flexibility exists in this aspect of the development.¹³

In the method originally proposed by Langhoff,⁹ $g(\epsilon)$ itself is approximated by a histogram obtained from the slopes of straight-line segments connecting the values of $\bar{F}^{(n)}(\epsilon_\alpha)$ given by Eq. (5). This defines the so-called Stieltjes derivative,

$$g(\omega_\alpha) \approx g^{(n)}(\omega_\alpha) = \frac{\bar{F}^{(n)}(\epsilon_{\alpha+1}) - \bar{F}^{(n)}(\epsilon_\alpha)}{\epsilon_{\alpha+1} - \epsilon_\alpha}, \quad (7)$$

at the succession of points

$$\omega_\alpha = \frac{1}{2} (\epsilon_\alpha + \epsilon_{\alpha+1}). \quad (8)$$

Alternatively, analytic forms can be fit to the discrete cumulative values $\bar{F}^{(n)}(\epsilon_\alpha)$ and differentiated to obtain a continuous approximation to $g(\epsilon)$. We found that, in the case of metastable neon, $\bar{F}^{(n)}(\epsilon_\alpha)$ could be adequately fit to a single exponential in ϵ plus a polynomial in $1/\epsilon$.

Some insight into the accuracy of the Stieltjes derivative values can be gained from the following consideration. Consider a Taylor series expansion of the exact cumulative oscillator strength about some point ϵ_0 in the continuum:

$$F(\epsilon) = F(\epsilon_0) + (\epsilon - \epsilon_0)F'(\epsilon_0) + \frac{1}{2}(\epsilon - \epsilon_0)^2 F''(\epsilon_0) \\ + \frac{1}{6}(\epsilon - \epsilon_0)^3 F'''(\epsilon_0) + \dots \quad (9)$$

If we now substitute this expansion into the Stieltjes derivative formula, Eq. (7), taking ϵ_0 to be the halfway point ω_α given in Eq. (8), then the even derivatives cancel and we obtain

$$g^{(n)}(\omega_\alpha) = F'(\omega_\alpha) + \frac{1}{24}(\epsilon_{\alpha+1} - \epsilon_\alpha)^2 F'''(\omega_\alpha) + \dots \quad (10)$$

Thus, the Stieltjes derivative will tend to overestimate the cross section in regions where the second derivative of the cross section, i.e., F''' , is positive and underestimate it in the reverse situation. As we will show in Sec. V, one can see this pattern in the present work when one compares the Stieltjes values with those obtained from a continuous, analytic fit to the calculated cumulative oscillator strength. This observation suggests that the latter procedure gives more reliable results.

More recently, Langhoff and Corcoran¹⁴ have suggested an alternative method for obtaining a continuous approximation to $g(\epsilon)$. The so-called Tchebycheff derivative is constructed by preassigning one of the energies at some desired point, ϵ_0 , and solving the moment problem for the remaining values $\{\epsilon_\alpha(\epsilon_0), f_\alpha(\epsilon_0)\}$, with this constraint. However, our experience in the case of metastable neon has been that, in order to obtain converged results, the Tchebycheff procedure requires a greater number of moments than the Stieltjes derivative. Consequently, in the present

work, we have used the latter method along with the analytic fit of the cumulative oscillator strength described earlier. We have generally found a range of n values over which mutually compatible cross sections were obtained.

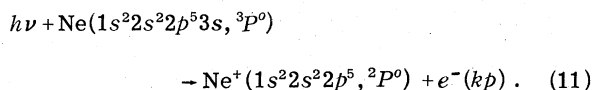
In actual numerical computations, we do not work with the power moments themselves, but rather with the set of recurrence coefficients $\{\alpha_n, \beta_n\}$ for the related orthogonal polynomials of the associated generalized quadrature problem. This procedure avoids the instabilities associated with working with the power moments themselves. These instabilities and their circumventions have been discussed in detail elsewhere^{14, 15} and will not be given here.

Experience gained from calculations on a number of atomic^{10, 14, 15} and molecular¹⁶⁻¹⁸ systems indicates that finite Hilbert-space calculations, which give N discrete energies and f values, can provide $2n$ accurate power moments for $n \ll N$. It is this observation which has led to a powerful computational procedure, since the input to moment-theory calculations can be obtained without resorting to numerical construction of continuum eigenstates.

III. CALCULATION OF THE ATOMIC WAVE FUNCTIONS

A. General comments

In this paper, we consider the ionization process:



In the LS coupling scheme, there are three allowed channels corresponding to $(1s^2 2s^2 2p^5 kp)$: ${}^3S^e$, ${}^3P^e$, and ${}^3D^e$. The first excited state of Ne^+ , $(1s^2 2s^2 2p^6, {}^2S^e)$ lies 26.9 eV above the ground state, so that there is a large energy region above the first ionization threshold where only the lowest ${}^2P^o$ state of Ne^+ is accessible. Although, in some of our calculations, we have included several excited states of Ne^+ as closed channels, we have not calculated the cross sections for ionization leading to excited states of Ne^+ .

In the present work, the initial bound state and the final continuum states are represented by linear superposition of many-electron configurations. Each configuration is an eigenstate of L^2 , L_z , S^2 , S_z , and parity, so that, in general, it must be a linear combination of Slater determinants. Each determinant is an antisymmetrized product of mutually orthogonal atomic orbitals (AO). The $1s$, $2s$, $3s$, and $2p$ AO's are taken from a self-consistent-field (SCF) calculation of the ${}^3P^o$ initial

state (see Sec. III B).^{19, 20} A $4d$ AO is obtained from a similar calculation of the $(2p^5 3d) {}^3P^o$ state of Ne. The other AO's are chosen either to span the lower rydbergs and the continuum, or to describe electron correlation in the $(2s^2 2p^5) {}^2P^o$ core. In most of our calculations we have used a basis set containing $4s$, $13p$, $4d$, and $2f$ AO's. For the ${}^3D^e$ final channel, where coupling to the $(2p^5 kf)$ continuum is possible,¹⁹ we have augmented the basis to $6f$ AO's.

The mutually orthogonal AO's are linear combinations of Slater-type orbitals (STO) which have the form:

$$\phi_i(\mathbf{r}) = \left(\frac{(2Z_i)^{2n_i+1}}{(2n_i)!} \right)^{1/2} r^{n_i-1} e^{-Z_i r} Y_{l_i m_i}(\hat{r}), \quad (12)$$

where $Y_{lm}(\hat{r})$ is a normalized spherical harmonic. Table I lists the parameters for our basis set con-

TABLE I. Ne Slater orbital parameters.^a

Orbital	n	l	Z
s_1	1	0	9.57 350
s_2	1	0	15.44 960
s_3	2	0	1.95 500
s_4	2	0	2.84 620
s_5	2	0	4.77 460
s_6	2	0	7.71 310
s_7	3	0	1.05 223
s_8	3	0	0.68 741
p_1	2	1	2.55 175
p_2	2	1	4.70 064
p_3	2	1	1.75 336
p_4	2	1	10.15 720
p_5	3	1	0.48 370
p_6	4	1	0.32 250
p_7	5	1	0.24 000
p_8	3	1	3.82 000
p_9	4	1	4.20 000
p_{10}	2	1	1.36 700
p_{11}	2	1	1.07 400
p_{12}	2	1	0.84 400
p_{13}	2	1	0.66 300
p_{14}	2	1	0.52 100
p_{15}	2	1	0.41 000
d_1	3	2	5.00 000
d_2	3	2	0.46 902
d_3	3	2	0.33 179
d_4	3	2	1.00 000
d_5	4	2	0.27 000
f_1	4	3	6.67 000
f_2	4	3	0.25 000
f_3	5	3	0.20 000
f_4	4	3	2.93 500
f_5	4	3	1.29 100
f_6	4	3	0.56 800

^aReferring to normalized Slater-type functions defined in Eq. (12) of the text.

taining 8s, 15p, 6d, and 6f STO's.¹⁹

In order to examine carefully the effects of core polarization and electron correlation on the photoionization cross section, we have calculated the many-electron wave functions describing the initial and the final states at four increasingly accurate levels of approximation. In the following, these wave functions will be referred to as: (i) the frozen-core wave function (FCW) (ii) the distorted-core wave function (DCW) (iii) The dipole-polarization wave function (DPW) (iv) The correlated wave function (CW). Each level of approximation will be discussed separately below.

B. Frozen-core approximation

In general, this approximation treats the ionization process as a one-electron problem by assuming that both the initial bound electron and the ejected electron move in the static-exchange potential of the frozen-core. The model assumes that the core does not relax during ionization. However, we wish to emphasize that, for systems with open-shell cores, the static-exchange potential is different in the initial and the final states. Because of the various possible angular momentum couplings between the core (with $j \neq 0$) and the additional electron, at least the exchange part of the core potential is different for states with distinct angular momentum quantum numbers.

In the frozen-core approximation, the initial ($1s^2 2s^2 2p^5 3s$) $^3P^0$ state of Ne is described by an SCF wave function. The calculated ionization potential of the $^3P^0$ state (relative to the SCF energy of Ne⁺) is 4.75 eV, whereas the experimental value is 4.89 eV. In the calculation of the final states, the 1s, 2s, and 2p AO's are "frozen," i.e., they are taken from the SCF calculation of the initial state. The final states are approximated by the expansion

$$\psi_f^{LS} = \sum_n C_n^{LS} (1s^2 2s^2 2p^5, ^2P^0) p_n, \quad (13)$$

where the $\{p_n\}$ are discrete, square-integrable p -type AO's, which are orthogonal to 2p. The expansion coefficients $\{C_n\}$ are determined by diagonalizing the full N -electron Hamiltonian for each value of L and S . Since the frozen core $1s^2 2s^2 2p^5$ is common to every term in the expansion (13), $\{C_n\}$ can be also obtained by diagonalizing the one-electron, static-exchange Hamiltonian of the 2P core in the basis $\{p_n\}$.

For the basis set of AO's described in Sec. IIIA, the lowest four eigenstates obtained in our calculations represented the ($2p^5 np$) rydberg states with $n=3-6$, while the remaining eight eigenvalues appeared in the continuum. The solutions

corresponding to these eigenvalues form the discrete, Hilbert-space representation of the continuum, from which one calculates the photoionization cross section via the Stieltjes procedure. A large number of p -type AO's must be included in the expansion (13) in order to describe, as accurately as possible, the kp continuum wave function associated with the long-range coulomb potential of the residual ion.

C. Distorted-core approximation

This approximation is intended to account for two effects which are absent in the FCW: the relaxation of the core upon ionization and the distortion of both the core and the outer orbitals due to incompletely filled subshells (mainly the 2p subshell in the present case of neon). The former is neglected in the FCW by definition. On the other hand, the spin and the angular polarization is neglected whenever one uses the restricted Hartree-Fock approximation (with maximum spin-pairing in doubly occupied orbitals) to describe configurations with open shells.²¹ For the process in Eq. (11) both the initial bound and the final continuum states contain two incompletely filled subshells. Thus, the static distortion of the SCF AO's could be important.

The distorted-core wave functions used in the present work are linear superpositions of configurations which include, in addition to the Hartree-Fock reference configurations, certain singly excited configurations allowed by symmetry. In particular, we include all types of single excitations from the 2s, 2p, and 3s AO's (or 2s, 2p, and kp AO's in the final state) to both occupied and some unoccupied AO's. The specific configurations are listed in the second column of Table II. The linear coefficients of the configurations are determined variationally by diagonalizing the full, many-electron Hamiltonian.

Although our one-electron basis set (see Sec. IIIA) contains only one "correlating" AO for each l value (\bar{s} , \bar{p} , \bar{d} , \bar{f}), the number of configurations in the final-state wave functions are rather large—between 176 and 377 configurations depending on the symmetry. This is due to the fact that each excitation out of the 2s and 2p AO's must be combined with every p -type AO used to expand the kp continuum function. In addition, some of the single excitations lead to configurations with as many as four incompletely filled subshells. Such a configuration may correspond to as many as nine linearly independent LS eigenfunctions. For example, the $2s - \bar{d}$ excitation leads to the spatial configuration $1s^2 2s 2p^5 p_n \bar{d}$. For a given AO p_n , there are nine linearly independent LS eigenfunctions assoc-

TABLE II. List of configurations used in the various approximations.^a

	FCW	DCW	DPW	CW
Initial	$2s^2 2p^5 3s^b$	$2s 2p^5 3s^2$	$2s 2p^6 kp$	
3P		$2s 2p^5 3s\bar{s}$	$2s 2p^5 kp\bar{p}$	$2p^5 3s\bar{s}^2$
		$2s 2p^5 3s\bar{d}$	$2s^2 2p^4 kp\bar{s}$	$2p^6 3s\bar{p}$
		$2s^2 2p^4 3s\bar{p}$	$2s^2 2p^4 kp\bar{d}$	$2s^2 2p^3 3s\bar{s}^2$
		$2s^2 2p^4 3s\bar{f}$	$2s^2 2p^4 3p 3d$	$2s^2 2p^3 3s\bar{p}^2$
		$2s^2 2p^5 3d$		$2s^2 2p^3 3s\bar{d}^2$
		$2s^2 2p^5 \bar{d}$		$2s 2p^4 3s\bar{s}\bar{p}$
Final	$2s^2 2p^5 kp$	$2s 2p^5 kp 3s$	$2s 2p^6 3s$	$2p^5 kp\bar{s}^2$
$^3S, ^3P, ^3D$		$2s 2p^5 kp\bar{s}$	$2s^2 2p^4 3s^2$	$2p^6 kp\bar{p}$
		$2s 2p^5 kp\bar{d}$	$2s^2 2p^4 3s 3d$	$2s^2 2p^3 kp\bar{s}^2$
		$2s^2 2p^4 kp\bar{p}$	$2s^2 2p^4 3s\bar{d}$	$2s^2 2p^3 kp\bar{p}^2$
		$2s^2 2p^4 kp\bar{f}$		$2s^2 2p^3 kp\bar{d}^2$
		$2s^2 2p^4 3p^2$		$2s 2p^4 kp\bar{s}\bar{p}$
		$2s^2 2p^5 kf^c$		

^aFor each level of approximation, the configurations appearing in that column were used in addition to the configurations in all previous columns.

^bThe doubly-occupied $1s$ AO is omitted for convenience, since no excitation out of this AO was used.

^cThese configurations contribute only to the 3D final channel.

iated with $(1s^2 2s 2p^5 p_n \bar{d})^3D$. Since we use a set of 12 p -type AO's to expand the kp continuum function, we must include 108 configurations in the wave function to represent the $2s \rightarrow \bar{d}$ excitation in the 3D final state.

In order to reduce the number of distinct Slater determinants in the wave functions and to make feasible calculations at higher levels of approximations (see Sec. III E), we included only those singly excited configurations in the final calculations which corresponded to a $^2P^o$ or a $^2S^o$ state of the Ne^+ core.²² Such a projection of the core is equivalent to neglecting the spin and angular, but not the radial, polarization of the core due to the outer $3s$ or kp electron. However, the relaxation of the core upon ionization, and the angular distortion of the active, outer electron due to the anisotropic core is properly described. As the discussion in Sec. IV will show, the difference between the cross sections obtained with the FCW and DCW arises mainly from the mixing of the $(1s^2 2s^2 2p^5 3s)$ and $(1s^2 2s^2 2p^5 3d)$ configurations in the initial state and is due to the angular distortion of the $3s$ electron.

In the 3D final channel, we have included the $(1s^2 2s^2 2p^5 kf)$ configurations in the DCW. In the frozen-core approximation, the oscillator strengths for the $3s \rightarrow nf$ or $3s \rightarrow kf$ transitions are zero by symmetry. However, in the DCW, the $(1s^2 2s^2 2p^5 kp)$ and the $(1s^2 2s^2 2p^5 kf)$ configurations are mixed slightly due to the angular distortion of the outer electron. Consequently, the "forbidden" $3s \rightarrow kf$ transitions "borrow" some intensity from the corresponding allowed $3s \rightarrow kp$ transitions.

D. Dipole-polarization wave function

As discussed in Sec. III C, the DCW accounts for the relaxation of the core during ionization and the static distortion of all the orbitals due to incompletely filled subshells. However, it still neglects the dynamic polarization of the core and the influence of this polarization on the motion of the outer electron. To account for the latter effect, it is necessary to add to the DCW a certain class of doubly excited configurations. In particular, the so-called dipole-polarization wave function (DPW) includes those doubly excited configurations which are connected by nonzero dipole matrix elements to the SCF reference configurations of the initial and the final states. The third column of Table II lists the specific configurations used. As before, the linear coefficients are determined by diagonalizing the many-electron Hamiltonian.

An inspection of Table II shows that the configurations in question involve the simultaneous excitation of the outer electron and one of the core electrons. Thus, in the language of quantum chemistry,²¹ these configurations involve "inter-shell double excitations" and contribute very little to the correlation energy because the outer and the core electrons occupy different regions of space. On the other hand, these configurations have an important effect on the bound-bound and bound-continuum oscillator strengths because they have relatively large dipole moment matrix elements with the SCF configurations. In addition, they correspond one-to-one to those core configurations which must be included in a calculation

of the dipole polarizability and the polarization potential of the Ne^+ core. Since we do not allow excitations out of the $1s$ AO, we neglect the small contribution of the $1s$ electrons to the polarizability of the core.

It should be noted that the doubly excited configurations included in the DPW for the final states constitute zeroth-order approximations to physical autoionizing states of Ne, which involve electrons loosely bound to the $(1s^2 2s 2p^6)^2 S^e$ and $(1s^2 2s^2 2p^4 3s)^4 P^e$ excited states of Ne^+ . The transitions between the 3P metastable state and these autoionizing states have large oscillator strengths, because the transition moments $\langle 2s | \vec{r} | 2p \rangle$, $\langle 2p | \vec{r} | 3s \rangle$ and $\langle 2p | \vec{r} | 3d \rangle$ are large. Thus, these autoionizing states should have a large effect on the total photoionization cross section of the 3P state just below the second ionization threshold at ~ 32 eV.

E. Correlated wave function

As a final improvement in the atomic wave functions, we have attempted to account for the most important electron correlation effects. Since the outer ($3s$ or kp) electron and the core electrons occupy different regions of space, pair correlation²¹ involving the outer electron is expected to be small. Furthermore, some of this correlation is already included in the DPW (see Sec. IIID). Thus, only the pair correlation of the core electrons needs to be added to the previous approximation. In order to identify the most important double excitations, we have carried out several configuration interaction (CI) calculations on the ground, $^2P^o$, state of Ne^+ , and used an energy criterion to select the configurations. Column 5 of Table II lists the doubly excited configurations used in the final calculations. As before, excitations out of the $1s$ AO were not considered. Although these excitations make a large contribution to the correlation energy, the magnitude of this contribution should be almost identical in the initial and the final states. Consequently, the correlation of $1s$ electrons should have only a small effect on the energies and the oscillator strengths for transitions involving the outermost electron.

The number of doubly excited configurations which must be included in the final-state wave functions is very large for the same reasons as discussed earlier in Sec. IIIC. Double excitations out of the core may lead to configurations with several open subshells, and, usually, such a configuration corresponds to many linearly independent LS eigenfunctions. For example, the excitation $2s 2p - \bar{s}\bar{p}$ leads to the spatial configuration $1s^2 2s 2p^4 k p \bar{s} \bar{p}$ with 5 incompletely filled AO's. Also, each excitation must be combined with every one

of the 12 p -type AO's used to expand the kp continuum function. In order to make the calculations with CW possible, we include only doubly excited, correlating, configurations in the final calculations, which correspond to a $^2P^o$ or a $^2S^o$ state of the Ne^+ core.²² In addition, several types of excitations, e.g., $2p^2 - \bar{s}\bar{d}$ and $2p^2 - \bar{f}^2$, are omitted entirely. Even with our basis of a few "correlating" AO's, the wave functions for some of the final states contained over 500 configurations (LS eigenfunctions) and as many as 5200 distinct Slater determinants. The CW used in the present work accounts for $\sim 45\%$ of the correlation energy of the electrons other than the $1s$ pair.

IV. RESULTS

A. Pseudospectra and the bound-bound transitions

Using the various wave functions described in Sec. III, we have calculated the transition energies and the oscillator strengths for the $(2p^5 3s)^3 P^o \rightarrow (2p^5 kp)^3 S^e, ^3P^e$, and $^3D^e$ transitions. We have evaluated both the dipole-length and the dipole-velocity forms of the transition moments. Since our calculations employ fully antisymmetrized, many-electron wave functions, one can use the extent of agreement between the dipole-length and dipole-velocity matrix elements to judge the accuracy of the results.

Table III gives a typical pseudospectrum which was obtained with the FCW for the $^3P^o - ^3D^e$ channel. For comparison, it also lists the experimental transition energies for several $3s \rightarrow np$ transitions. An inspection of Table III shows that

TABLE III. Pseudospectrum calculated with the FCW for the transitions $(2p^5 3s)^3 P^o \rightarrow (2p^5 kp)^3 D^e$ in Ne. The calculated value for the first ionization threshold is 0.1745 a.u. $A - n$ stands for $A \times 10^{-n}$.

Final state	$\Delta E_{\text{expt.}}^a$	ΔE^b	Length	f Velocity
$3p$	0.0697	0.0664	5.45-1	5.42-1
$4p$	0.1285	0.1248	4.95-3	4.37-3
$5p$	0.1495	0.1459	4.91-4	4.41-4
$6p$	0.1596	0.1587	1.93-4	1.73-4
k_{1p}	...	0.1882	3.40-6	4.66-6
k_{2p}	...	0.2605	1.31-3	1.44-3
k_{3p}	...	0.4217	4.67-3	5.07-3
k_{4p}	...	0.7866	7.09-3	7.08-3
k_{5p}	...	1.6587	6.90-3	6.44-3
k_{6p}	...	3.8965	5.80-3	5.17-3
k_{7p}	...	9.9306	3.90-3	3.28-3
k_{8p}	...	34.4594	1.49-3	1.44-3

^a Transition energies for $^3P^o - ^3D^e$.

^b Energies in atomic units (1.0 a.u. = 27.21 eV).

the four lowest solutions correspond to the $(2p^5np)$ rydberg states with $n=3-6$ and that the calculated transition energies are reasonably accurate. The remaining eight solutions form a discrete representation of the ionization continuum. Our choice of the 12 p -type AO's (see Sec. IIIA) leads to four eigenvalues between the first and second ionization thresholds, at 0.175 and 1.163 a.u. respectively. As we will show in Sec. IV B, Stieltjes imaging of such a distribution of points in the pseudospectrum produces converged photoionization cross sections from threshold to about 1.0 a.u. Our experience indicates that one must use a sufficiently large one-electron basis set in order to obtain a spectrum which is dense enough to produce converged results in energy regions where the cross section has structure and is not monotonic.²³

We wish to emphasize that the pseudospectrum which is shown in Table III for the case of $^3P^o \rightarrow ^3D^e$ is quite typical; similar distributions of eigenvalues were obtained for $^3P^o \rightarrow ^3S^e$ and $^3P^o \rightarrow ^3P^e$. Furthermore, inclusion of core polarization and electron correlation in the wave functions introduced no new eigenvalues below 1.0 a.u. and left the nature of the spectrum in this region essentially unchanged. When the calculations were performed with the DPW and CW (which include doubly excited configurations), autoionizing states did appear in the spectrum between 1.05 and 2.0 a.u. A discussion of how these autoionizing states were treated in the Stieltjes calculation of the photoionization cross section will be deferred to Sec. IV B.

Next, we compare briefly the available experimental and theoretical oscillator strengths for bound-bound transitions originating from the 3P metastable states of Ne. Such a comparison is complicated by the fact that, while the excited states of neon are characterized by $j-l$ coupling, our calculations were done in LS coupling. However, for certain symmetries, it is possible to find states which are pure LS states, provided interactions with other, high-lying configurations are neglected. One example is the $(2p^53s)^3P_2 \rightarrow (2p^5np)^3D_3$ series, because the configurations $(2p^53s)$ and $(2p^5np)$ lead to only one $J=2$, and one $J=3$ state, respectively. Table IV compares our calculated line strengths to the experimental and other theoretical values for the first two transitions ($n=3, 4$) of this series. For the strong $3s \rightarrow 3p$ transition, theory and experiment^{24, 25} agree within 10%, although our calculated values are systematically too high. For the much weaker $3s \rightarrow 4p$ transition, there is reasonable agreement between our values and that calculated by Starace using the one-electron Coulomb approximation.²⁶

TABLE IV. Comparison of experimental and theoretical line strengths (in atomic units) for the two lowest $(2p^53s)^3P_2 \rightarrow (2p^5np)^3D_3^e$ transitions in neon.

	3p	4p
Present theory: FCW ^a	51.8	0.25
Present theory: CW ^a	51.1	0.23
Coulomb approximation ^b	47.2	0.27
Intermediate coupling ^c	...	0.13
Experiment ^d	45.9 ± 3.2	...
Experiment ^e	48.9	...
Experiment ^f	...	1.4 ± 0.4

^a Calculated with the "dipole-length" matrix elements.

^b Reference 26.

^c Reference 27.

^d Reference 24.

^e Reference 25.

^f References 28 and 29.

Intermediate coupling theory²⁷ appears to give too small a value for this transition. The value extracted by Wiese *et al.*²⁸ from lifetime measurements²⁹ is definitely incorrect.

Finally, we note that using the calculated pseudospectrum, one can easily determine the static dipole polarizability of the initial state. In fact, this is done automatically in the Stieltjes procedure, because the static polarizability is just the second inverse moment of the oscillator strength distribution, i.e., it is $S(-2)$ which appears in Eq. (4). The experimental value³⁰ for the average polarizability of the $(2p^53s)^3P$ state of Ne is $27.8 \pm 0.6 \text{ \AA}^3$. Our best calculations with CW yield 30.7 \AA^3 (dipole length) and 27.5 \AA^3 (dipole velocity). The discrepancy between the latter two values is due to small errors ($\approx 0.05 \text{ eV}$) in the computed transition energies for the $3s \rightarrow 3p$ transitions which carry large oscillator strengths. In fact, over 98% of the polarizability of the $(2p^53s)^3P$ state is due to the $3s \rightarrow 3p$ transitions. A completely analogous result was obtained by Kelly³¹ for the polarizability of the $(2p^33s)^5S^o$ state of atomic oxygen.

B. Photoionization cross sections

We have evaluated the photoionization cross sections from the power moments of the calculated pseudospectra using either the Stieltjes derivative formula, Eq. (7), or continuous, analytic fits of the cumulative oscillator strength distributions. Figure 1 compares the results which we have obtained with these two procedures for a typical case, the $(2p^53s)^3P \rightarrow (2p^5kp)^3D$ channel. (The corresponding pseudospectrum calculated with the FCW is displayed in Table III). Two features of these results are noteworthy. First, the Stieltjes

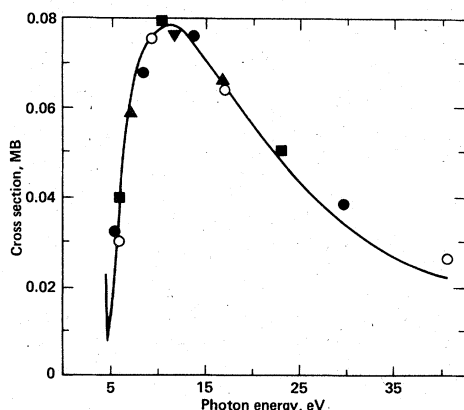


FIG. 1. Partial photoionization cross section for $^3P \rightarrow ^3D$ channel obtained with frozen-core wave functions (FCW). Solid curve: cross section obtained with analytic fit of cumulative function $F(\epsilon)$ [Eq. (1)]. Individual points represent Stieltjes derivative values [Eq. (7)] obtained with the first n moments: ∇ , $n=10$; Δ , $n=12$; \blacksquare , $n=14$; \bullet , $n=16$; \circ , $n=18$.

values of the cross section which we have calculated using different sets of moments fall on a reasonably smooth curve. This shows that our basis of p -type AO's is sufficiently large, and the resulting pseudospectrum is sufficiently dense, to provide converged cross section between threshold and about 30 eV. Second, in our discussion of the Stieltjes procedure (see Sec. II), we remarked that the Stieltjes derivative, being a linear approximation, tends to overestimate the cross section where the curvature of the cross section is positive, and to underestimate in the opposite case. This behavior is clearly visible in Fig. 1, especially for $E > 15$ eV. We emphasize here that the results shown in Fig. 1 are typical; very similar

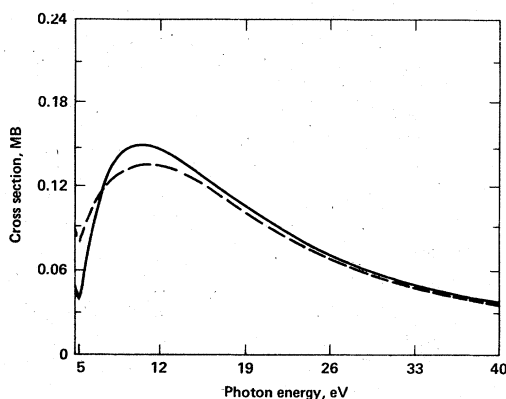


FIG. 2. Total photoionization cross section for $(2p^5 3s)^3P$ state obtained with frozen-core wave functions (FCW). Solid curve: dipole velocity form; dashed curve: dipole length form.

plots were obtained for the other two channels and with the more elaborate wave functions. In the present calculations we have found that, for our basis of p -type AO's the Stieltjes derivative formula and the analytic fit of $F(\epsilon)$ gave mutually compatible results when we used the first 10–18 moments of the calculated oscillator strength distributions. Since the latter method requires no approximation for the derivative and gives the cross section for any energy, it was used to obtain the results which are presented in the remainder of this section.

Since the various atomic wave functions used in the present work were calculated in the presence of nonlocal exchange interactions, their accuracy can be judged from the degree of agreement (or disagreement) between the cross sections computed with the dipole-length and the dipole-velocity forms of the transition moment. Figure 2 shows the total photoionization cross sections which we have obtained for the $(2p^5 3s)$ state of neon with the FCW. It is clear that the "length" and the "velocity" forms of the cross section differ significantly from threshold to about 15 eV. At threshold, the two cross sections differ by a factor of 2. In the case of the $^3P \rightarrow ^3P$ and $^3P \rightarrow ^3S$ partial cross sections, the discrepancy is even greater than what Fig. 2 shows, about 60% at peak value.

In Fig. 3 we compare the total cross sections ("velocity" form) which we have calculated using the four levels of approximation discussed in Sec. III. In going from the frozen core (FCW) to the distorted core (DCW) approximation, the peak values of the "length" and the "velocity" cross sections increase by 20% and 30%, respectively.

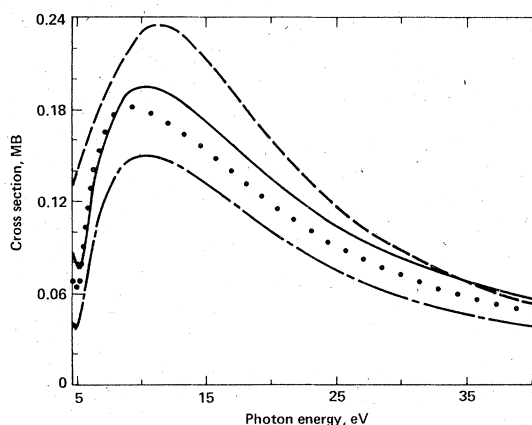


FIG. 3. Comparison of the total photoionization cross sections ("velocity" form) calculated with four different approximations. Solid curve: correlated wave function (CW); dashed curve: (DPW); dotted curve: distorted core wave function (DCW); dot-dashed curve; frozen core wave function (FCW).

By carefully repeating the DCW calculations using slightly different sets of singly excited configurations, we have found that most of the increase in the "velocity" cross section is due to the relaxation of the core orbitals during ionization. On the other hand, the increase in the "length" form is due almost entirely to the angular polarization of the 3s electron in the initial state. Figure 3 also shows that, in going from the distorted core wave function (DCW) to the dipole-polarization wave function (DPW), the peak value of the total cross section ("velocity" form) increases by another 30%. This increase is due largely to the presence of those doubly excited configurations in the final state which have nonzero dipole matrix elements with the reference configuration of the initial state. As discussed in Sec. IIID, these doubly excited configurations correspond to physical autoionizing states which are connected to the initial $(2p^5 3s)^3P$ state by large oscillator strengths. Thus, even relatively small mixing of these autoionizing states into the nonresonant $(2p^5 kp)$ continua leads to significant increases in the continuum oscillator strength far away from the autoionization region near the second ionization threshold. Finally, in going from the dipole polarization (DPW) to the correlated wave functions (CW), the peak value of the total cross section decreases by about 20% (see Fig. 3). This change can be understood by recognizing that the CW contains a large number of doubly excited configurations which have vanishing dipole-matrix elements with the reference configurations of the initial and the final states. The inclusion of such double excitations in the calculations decreases the linear coefficients of the reference configurations in the CI wave functions. This, in turn, results in a decreasing contribution of the SCF configurations to the transition moments.

Next, we discuss briefly how the autoionizing (AI) states were treated in our calculations. The results in Fig. 3 clearly show that polarization and electron-electron correlation influence the shape and the magnitude of the photoionization cross section of metastable neon. In order to account for these effects, one must include in the wave functions singly and doubly excited configurations, some of which represent physical autoionizing states. Some of these AI states, e.g., $(2s2p^6 3s)^3S^e$, carry large oscillator strengths from the initial $(2s^2 2p^5 3s)^3P^o$ state, while others, e.g., $(2s^2 2p^4 3p^2)^3S^e$, are nearly forbidden. In the AI region, the resulting pseudospectra may contain closely spaced points with very different oscillator strengths. If one attempts to use such a pseudospectrum (with rapidly varying oscillator strengths) in the Stieltjes procedure, wildly oscillating and physically meaningless photoioniza-

tion cross sections result.^{15, 16} In order to avoid this difficulty in our calculations, we inspected the eigenvector associated with every eigenvalue of the Hamiltonian. By examining the contributions of the various configurations to each wave function, we were able to identify each solution as representing *either* the $(2s^2 2p^5 kp)$ continuum, *or* another continuum associated with an excited state of Ne^+ , e.g., $(2s^2 2p^4 3s kd)$, *or* a physical autoionizing state. Only those solutions which had large contributions from the frozen-core $(2s2p^5 np)$ configurations and which therefore corresponded to the nonresonant continuum, were included in the Stieltjes moment analysis. (Such an inspection of the CI wave functions is very similar to the procedure used in the stabilization method³² for calculating resonances, e.g., AI states, where one looks for those solutions which have large contributions from spatially localized configurations.)

In neon, the lowest AI state with even parity is probably the $(2s2p^6 3s)^3S^e$ state which is located about 28 eV above the $(2s^2 2p^5 3s)^3P^o$ state. Thus, for photon energies greater than 28 eV, AI states will contribute to the total ionization signal. Since we have not included these AI states in the Stieltjes procedure, our calculated total cross sections above 28 eV represent only direct ionization leading to the $(2s^2 2p^5)^2P^o$ state of the ion. Furthermore, above the second ionization threshold, at 31.8 eV, our cross sections do not include the contribution of direct ionization leading to the $(2s2p^6)^2S^e$ state of Ne^+ .

Figure 4 displays our final results for the photoionization of metastable neon which we have obtained with the CW. The individual partial cross sections: $^3P \rightarrow ^3S$, $^3P \rightarrow ^3P$, and $^3P \rightarrow ^3D$, as well as the total cross section are shown for both the

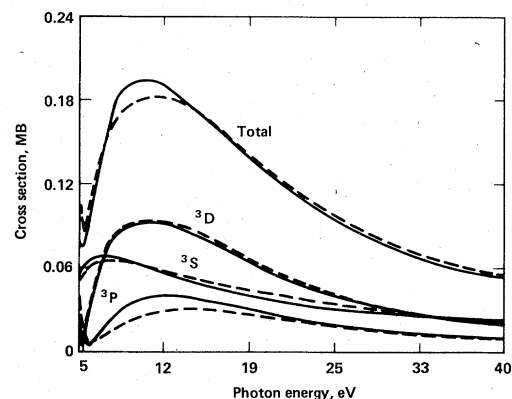


FIG. 4. Partial and total photoionization cross sections for $(2p^5 3s)^3P \rightarrow (2p^5 kp)^3S$, 3P , 3D calculated with correlated wave functions (CW). Solid curves: dipole velocity form; dashed curves: dipole-length form.

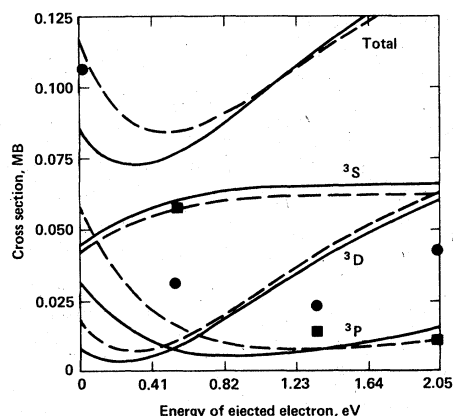


FIG. 5. Partial and total photoionization cross sections for $(2p^5 3s)^3P \rightarrow (2p^5 kp)^3S$, 3P , 3D in the threshold region. Solid curves: dipole velocity form; dashed curves: dipole-length form. Individual points represent values calculated by Hartquist (Ref. 8) for the 3P_J initial states: \bullet , $J=0$; \blacksquare , $J=2$.

“length” and “velocity” forms of the transition moment. A comparison of Figs. 2 and 4 shows that using correlated wave functions in the calculations improved significantly the agreement between the “length” and the “velocity” cross sections, especially near threshold. It is clear that the remaining discrepancy is due almost entirely to the $^3P \rightarrow ^3P$ cross section which has the smallest magnitude among the three. The agreement between the two forms of the cross section is excellent over a wide energy range for the $^3P \rightarrow ^3S$ and $^3P \rightarrow ^3D$ channels.

The behavior of the cross section near threshold is interesting because of the appearance of the “Cooper minimum.”³³ Figure 5 shows the near-threshold region in more detail. One of the striking features is that the minimum in the $^3P \rightarrow ^3S$ oscillator strength evidently occurs among the discrete $3s \rightarrow np$ rydberg transitions. We obtained the same result at *every level* of approximation, although the exact location of the minimum and the threshold value of the photoionization cross section varied somewhat.

In a simple, one-electron picture of ionization, the minimum value of the partial cross sections (in the 3P and 3D channels) should be zero. The fact that our calculated minima are small but finite is due partly to many-electron correlation effects and partly to some inaccuracy in fitting the cumulative oscillator strengths to analytic forms. In the various channels, the minima occur at different energies because the $(2s^2 2p^5) \text{Ne}^+$ core is not spherically symmetric, and therefore the potential seen by the ionized electron depends on the total orbital angular momentum L . The practical con-

sequence of this fact is that the minimum in the total cross section is not as deep as those in the individual partial cross sections.

Finally, we compare our results to previous work. Figure 5 shows the values of the cross sections for the 3P_0 and 3P_2 levels of neon which have been calculated by Hartquist⁸ using the quantum defect method. A detailed comparison is difficult because his results refer to states described by $j_{\text{core}} - j$ coupling, whereas we have used LS coupling and neglected the spin-orbit splitting in the $^2P^o$ state of Ne^+ (~ 0.1 eV). If the latter assumption is justified, our calculated cross sections should be valid for the 3P_0 and 3P_2 (but not the 3P_1) states, because these are pure LS states provided mixing with other higher-lying states is negligible. We feel that neglecting the splitting between the $j = \frac{1}{2}$ and $j = \frac{3}{2}$ states of Ne^+ should have only a small effect on the cross sections for ejected electron energies greater than 1.0 eV. Considering all these assumptions, we find that our values of the cross sections at threshold are the same order of magnitude as those of Hartquist,⁸ but the energy dependence is quite different.

Figure 6 compares our total photoionization cross section to that calculated by McCann and Flannery,⁷ who used a one-electron model potential to describe the initial and the final states of the active electron. The magnitude of the cross sections are quite similar over a wide energy range between 10 and 40 eV. In this region, our results are somewhat larger due to the inclusion of many-electron effects in the calculations. On the other hand, the difference between the calculated cross sections is quite large from threshold to 10 eV: the cross section of McCann and Flannery

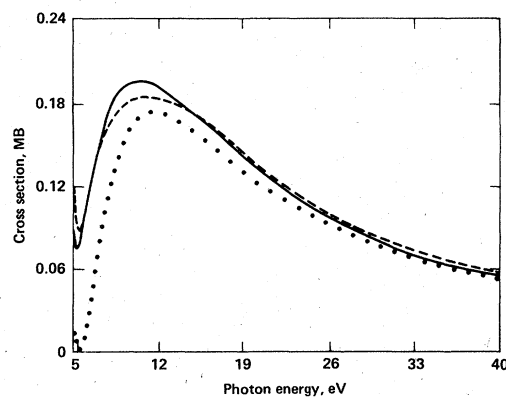


FIG. 6. Comparison of calculated total photoionization cross sections for $(2p^5 3s)^3P \rightarrow (2p^5)^2P + e^-$. Solid curve: present result—“velocity” form; dashed curve: present result—“length” form; dotted curve: result of McCann and Flannery (Ref. 7).

nery actually dips to zero and their threshold value is a factor of 10 smaller. The former is due to the fact that these authors averaged their atomic potential over the various angular momentum couplings which are possible between the open-shell 2P state of the core and the active kp electron. (See the discussion of Fig. 5 earlier). The results presented in Fig. 6 lead to the conclusion that orbital relaxation, polarization, and electron correlation effects are important in determining the magnitude of the photoionization cross section from threshold to about 5 eV (ejected electron energy).

V. SUMMARY AND CONCLUSIONS

In the present work, we have calculated the photoionization cross section for the $(1s^22s^22p^53s)-^3P$ metastable state of Ne using *ab initio*, many-electron wave functions in the *LS*-coupling scheme. We have considered all open channels which correspond to the $(1s^22s^22p^5)^2P$ state of Ne^+ and an ejected p electron. Although several excited states of Ne^+ were included in the calculations as closed channels, we have not determined the cross section for processes leading to excited states of the ion.

The $(1s^22s^22p^5kp)$ continua were discretized by approximating the final-state wave functions as superpositions of square-integrable configurations. In order to examine the effects of orbital relaxation, core polarization, and electron correlation, the initial and the final states were calculated at four increasingly accurate levels of approximation. The shape and the magnitude of the cross section within 5 eV of threshold were found to depend sensitively on these effects. The accuracy of the various wave functions was judged from the degree of agreement between the dipole-length and the dipole-velocity forms of the cross sections. We have used the Stieltjes moment-theory technique to construct the continuum oscillator strength distribution from the calculated pseudospectra of discrete transition energies and oscillator strengths. The cross sections were computed from the cumulative oscillator strengths using either the so-called Stieltjes derivative or continuous, analytic fits of the cumulative function, $F(\epsilon)$. In order to obtain converged cross sections from threshold to 30 eV, we found it necessary to use a sufficiently large one-electron basis for the ionized electron which led to a rea-

sonably dense spectrum between the first and the second thresholds.

In order to account for polarization and correlation effects, we had to include in the final-state wave functions doubly excited configurations which corresponded to physical autoionizing states. Often, the presence of such states in the pseudospectrum used in the Stieltjes procedure can lead to anomalous behavior of the photoionization cross section as a function of energy. In order to avoid this problem in our calculations, we have included in the moment analysis only those eigenvalues of the Hamiltonian matrix which had large projections on the non-resonant continuum $(2s^22p^5kp)$. Thus, our calculated cross sections do not include any contributions from autoionization. In the present case of metastable neon, this a workable procedure because excitation out of the $(1s^22s^22p^53s)^3P$ state leads to essentially a one-electron spectrum with widely spaced ionization thresholds. It should be recognized that the same procedure may not work in other cases where there are nearly degenerate thresholds, or where there are several strongly coupled open channels. Furthermore, the direct inclusion of autoionizing states in the Stieltjes moment analysis is still a difficult problem which needs further theoretical study.

We have compared our calculated photoionization cross sections to the results of other workers. The threshold value of the cross section, $1.0 \times 10^{-19} \text{ cm}^2$, is in reasonable agreement with that obtained by Hartquist,⁸ but it is almost a factor of 10 larger than the value of McCann and Flannery.⁷ The peak value of the cross section, $1.9 \times 10^{-19} \text{ cm}^2$, is somewhat larger than that calculated by McCann and Flannery.

The application of the present computational procedure to the photoionization of the metastable states of the heavier rare gases will require the explicit consideration of spin-orbit coupling. Currently, we are investigating the inclusion of this effect in a Stieltjes calculation of the photoionization cross section.

ACKNOWLEDGMENTS

We are grateful to Dr. McCann, Dr. Flannery, and Dr. Hartquist for sending us their results prior to publication. We thank Professor Ernest Davidson for helpful discussions on aspects of atomic configuration-interaction calculations.

*Work performed under the auspices of the U. S. ERDA under Contract No. W-7405-Eng-48.

¹C. K. Rhodes, IEEE J. Quantum Electron. QE-10, No. 2, 153 (1974).

²B. W. Shore, J. Phys. B 8, 2023 (1975), and references cited therein.

³D. W. Norcross, J. Phys. B 4, 652 (1971); V. L. Jacobs, Phys. Rev. A 9, 1938 (1974).

- ⁴A. Dalgarno, H. Doyle, and M. Oppenheimer, *Phys. Rev. Lett.* **29**, 1051 (1972).
- ⁵T. N. Rescigno, C. W. McCurdy, and V. McKoy, *J. Chem. Phys.* **64**, 477 (1976).
- ⁶M. Aymar, E. Luc-Koenig, and F. Combet Farnoux, *J. Phys. B* **9**, 1279 (1976), and references cited therein.
- ⁷K. J. McCann and M. R. Flannery, *App. Phys. Lett.* **31**, 599 (1977).
- ⁸T. Hartquist (unpublished).
- ⁹(a) P. W. Langhoff, *Chem. Phys. Lett.* **22**, 60 (1973);
(b) P. W. Langhoff and C. T. Corcoran, *J. Chem. Phys.* **61**, 146 (1974); (c) P. W. Langhoff, J. Sims, and C. T. Corcoran, *Phys. Rev. A* **10**, 829 (1974).
- ¹⁰P. W. Langhoff, *J. Chem. Phys.* **57**, 2604 (1972).
- ¹¹J. A. Shohat and J. D. Tamarkin, *The Problem of Moments, Mathematical Surveys* 1 (American Mathematical Society, Providence, 1943).
- ¹²U. Fano and J. W. Cooper, *Rev. Mod. Phys.* **40**, 441 (1968).
- ¹³The generation of a continuous representation of the cross section through polynomial fits to discrete Stieltjes values is discussed in Ref. 9c. Alternatively, the use of cubic natural spline functions to fit the discrete cumulative values $\bar{F}^{(n)}(\epsilon_a)$ has been discussed by Nesbet (see Ref. 15). A rather different interpolation scheme, based on the so-called Heller derivative for smoothly interpolating Gaussian abscissas [E. J. Heller, thesis (Harvard University, 1973) and also P. L. Altick, *Phys. Rev. A* **10**, 1003 (1974)] has been used in an H^- photodetachment study by J. T. Broad and W. P. Reinhardt, *Chem. Phys. Lett.* **37**, 212 (1976).
- ¹⁴(a) P. W. Langhoff and C. T. Corcoran, *Chem. Phys. Lett.* **40**, 367 (1976); (b) P. W. Langhoff, C. T. Corcoran, J. S. Sims, F. Weinhold, and R. M. Glover, *Phys. Rev. A* **14**, 1042 (1976); (c) C. T. Corcoran and P. W. Langhoff, *J. Math. Phys.* **18**, 651 (1977).
- ¹⁵R. K. Nesbet, *Phys. Rev. A* **14**, 1065 (1976).
- ¹⁶T. N. Rescigno, C. F. Bender, V. McKoy, and P. W. Langhoff, *J. Chem. Phys.* (to be published).
- ¹⁷P. W. Langhoff, S. R. Langhoff, and C. T. Corcoran, *J. Chem. Phys.* **67**, 1722 (1977).
- ¹⁸S. V. O'Neil and W. P. Reinhardt (unpublished).
- ¹⁹The various STO's were chosen in the following manner. The functions s_1-s_6 and p_1-p_7 were taken from the basis sets of Clementi and Roetti (Ref. 20) for Ne and Ne^+ , respectively. The functions s_7 and s_8 were optimized in the SCF calculation of the $(2p^5 3s)^3P^o$ state. The functions p_8-p_{15} were chosen to represent the $3p$, $4p$, and $5p$ rydberg states, while the remaining p -type STO's ($p_{16}-p_{19}$) were chosen to span r space between the maxima of the $2p$ and $3p$ AO's. The functions d_1 and f_1 were designed to describe the angular polarization of the $2s$ and $2p$ electrons, respectively. The functions d_2 and d_3 were optimized in the SCF calculation of the $2p^5 3d^3P^o$ state. The remaining d - and f -type STO's were selected to span the rydbergs and the continuum.
- ²⁰E. Clementi and C. Roetti, *At. Data Nucl. Data Tables* **14**, 177 (1974).
- ²¹H. F. Schaefer, *The Electronic Structure of Atoms and Molecules* (Addison-Wesley, Reading, Mass., 1972).
- ²²Such projections within degenerate subspaces of open-shell systems have been studied previously in CI calculations of atoms. See A. Bunge, *J. Chem. Phys.* **53**, 768 (1970).
- ²³In cases where the photoionization cross section is a monotonic function of energy, a sparser pseudospectrum may be sufficient to give accurate results. Nesbet, in his recent calculation on helium and boron (Ref. 15) used smaller basis sets for the ionized electron and obtained sparser pseudospectra below the onset for autoionization. Nevertheless, his calculated cross section for He compares favorably with the experimental data.
- ²⁴J. M. Bridges and W. L. Wiese, *Phys. Rev. A* **2**, 285 (1970).
- ²⁵E. Koenig, *Phys. Lett.* **34A**, 284 (1971).
- ²⁶A. F. Starace, *J. Phys. B* **6**, 76 (1973).
- ²⁷R. A. Lilly, *J. Opt. Soc. Am.* **65**, 389 (1975).
- ²⁸W. L. Wiese, M. W. Smith, and B. M. Glennon, *Atomic Transition Probabilities*, Vol. 1 (U.S. GPO, Washington, D. C., 1966).
- ²⁹J. Z. Klose, *Phys. Rev.* **141**, 181 (1966).
- ³⁰R. W. Molof, H. L. Schwartz, T. M. Miller, and B. Bederson, *Phys. Rev. A* **10**, 1131 (1974).
- ³¹H. P. Kelly, *Phys. Rev.* **152**, 62 (1966).
- ³²H. S. Taylor and A. U. Hazi, *Phys. Rev. A* **14**, 2071 (1976).
- ³³J. W. Cooper, *Phys. Rev.* **128**, 681 (1962); U. Fano and J. W. Cooper, *Rev. Mod. Phys.* **40**, 441 (1968).